A new take on porous medium approach for modelling monoliths and other multiple channel devices

Padula, G, Saul, J, Aleksandrova, S, Medina, H & Benjamin, S

ISSN 0148-7191
ESSN 2688-3627
Publisher: SAE International

A new take on porous medium approach for modelling monoliths and other multiple channel devices

Author, co-author (Do NOT enter this information. It will be pulled from participant tab in MyTechZone)

Affiliation (Do NOT enter this information. It will be pulled from participant tab in MyTechZone)

Abstract

The porous medium approach is widely used to represent high-resistance devices, such as catalysts, filters or heat exchangers. Because of its computational efficiency, it is invaluable when flow losses need to be predicted on a system level. A drawback of using the porous medium approach is the loss of detailed information downstream of the device. Correct evaluation of the turbulence downstream affects the calculation of the related properties, e.g. heat and mass transfer.

The approach proposed in the current study is based on a modified distribution of the resistance across the porous medium, which allows to account for the single jets developing in the small channels, showing an improved prediction of the turbulence at the exit of the device, while keeping the low computational demand of the porous medium approach.

The benefits and limitations of the current approach are discussed and presented by comparing the results with different numerical approaches and experiments. The flexibility of the proposed approach in terms of describing the device geometry is demonstrated via an optimisation study where the size of the monolith channels is modified to obtain a more uniform distribution of the flow.

The approach is applied to a monolith commonly used in automotive exhaust after-treatment systems, but can be generalized to other high resistance devices with multiple channels.

Introduction

The numerical studies of devices with high resistance, such as heat exchangers and automotive catalysts, are commonly performed by modelling the channels and tubes as a distributed resistance, in analogy with the flow model of a porous medium [1]. Including detailed geometry of such devices is, indeed, impractical because of the high computational requirements, since multiple scales need to be modelled, from the molecular scale to the converter scale [2]. On the other hand, accurate prediction of turbulence inside and downstream of the porous medium is crucial to determining correlated properties, such as heat transfer and flow diffusion [3].

Numerical models are widely used to design the components and optimise parameters of the after-treatment systems in industry [4]. Since the after-treatment system often consists of multiple devices used in series, it is crucial to correctly predict the flow both upstream and downstream of each device.

The use of a distributed resistance approach to model this class of devices allows to significantly reduce the computational time requirements, while providing sufficient information about the mean flow and pressure distribution. Several studies have shown a good prediction of the downstream velocity distribution [5, 6].

In order to define the porous medium resistance coefficients, experimental data or semi-empirical laws developed for single channels [7] are commonly applied to 2D or 3D models [8, 9]. A good agreement with the experimental results can be achieved, with an acceptable accuracy, especially during the design phase.

The key limitation of the porous medium approach is the prediction of the turbulence downstream the device. In the case of a monolith used in automotive applications, for example, the single jets exiting the channels can be unstable and generate turbulent structures [10]. Flow transition from a laminar to turbulent regime has been observed inside packed beds, with a direct impact on the prediction of the heat transfer properties [11]. Modelling full scale geometry, including individual channels, has been tested for 2D models [6, 9], but can be prohibitive in terms of computational requirements for a 3D case.

To address the problem of turbulence damping by the porous medium models, modified RANS models have been introduced to account for different scales of the flow inside a porous medium [12]. In another study, the use of artificially generated turbulence downstream has been proposed [10]. Such approaches increase the computational cost of the simulation when compared to a porous medium model, limiting the applicability of the model to more general configurations and devices.

The approach suggested in the current study is based on a modified function for the resistance across the porous medium, based on the geometry of the system adopted. It offers flexibility in terms of geometry description and better prediction of the flow properties downstream, while keeping the computational cost low.

In order to demonstrate how the porous medium approach can be used for geometry optimisation, an algorithm to optimise the flow distribution in the device has been tested and is proposed in the last section of the paper. The size of the channels is modified in order to achieve a uniform velocity distribution exiting the monolith, with a consequent reduction of the pressure losses.

Ability to modify the porous medium geometry easily can be useful when designing multi-channel devices. The application of 3D printing technology to the production of catalysts and filters is a promising technique that allows to vary the dimensions of the channels [13, 14], previously obtained by extrusion [15]. This

technology, when mature, will allow to create customised geometry devices with channel size design based on the distribution of the flow entering the device, allowing the production of optimized monoliths with high uniformity indices.

Methodology

A two-dimensional geometry with a diffuser upstream of a catalyst monolith has been adopted for the current study, for both experimental and numerical activities (Figure 1). This geometry has been previously used in the experimental and numerical study of Porter et al. [6], therefore a good database is available for comparison. The domain consists of three regions, namely the diffuser (1), the monolith (2) and the outlet sleeve (3). Note that due to symmetry only half of the geometry is considered in the simulations, with y = 0 being the symmetry plane.

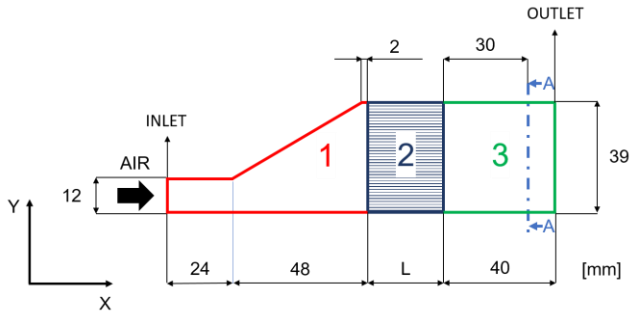

Figure 1. Schematic representation of the domain: diffuser region (1), monolith (2) and outlet sleeve (3). Dimensions in mm. Only top half of the geometry is shown.

Experiments

The measurements used to validate the current model have been published in the study by Porter et al. [6].

A "planar" diffuser was attached to a catalyst monolith with square channels with channel hydraulic diameter of 1.12 mm and cell density of 62 cells/cm^2. Two monolith lengths have been used (L_1 = 27 mm and L_2 = 100 mm) with different inlet mass flow rates, resulting in Reynolds numbers from Re=22000 to Re=60000 based on the inlet hydraulic diameter of the geometry (38.4 mm) and a mean velocity at the inlet pipe (about 9 m/s and 24.5 m/s, respectively). The velocity at a cross-section 30 mm downstream the monolith (section A-A in Figure 1) has been sampled using a single hot-wire probe normal to the section. It was established that the flow was nearly two-dimensional (z-independent) away from the side walls of the diffuser. Further details of the experiments can be found in [6].

In order to determine the resistance coefficients needed for modelling the porous medium section of the monolith, pressure losses in the monolith in a uniform axial flow have been measured in separate experiments, also described in [6].

Numerical approach

A 2D numerical model has been implemented in StarCCM+ v.12, using the RANS v2f approach to model turbulence. The domain has been discretised using hexahedral cells combined with prism cell layers at the wall boundaries. A structured mesh is therefore used throughout the entire domain.

The monolith region has been treated as a porous medium. A condensed monolith approach, discussed in the following section, has been used to reduce the number of computational cells required by the numerical simulation.

A mesh independence study has been carried out for the highest Reynolds number considered (Re=60000), monitoring some parameters of interest, such as pressure drop and outlet velocity. The maximum difference in pressure drop prediction and maximum velocity at the outlet between the selected mesh and the most refined mesh has been calculated to be less than 1%, while the computational time was about 30% higher.

Monolith model

The monolith consists of multiple channels with small hydraulic diameters. Modelling individual channels is very computationally expensive, as thin boundary layers have to be resolved in each channel. Therefore, various alternative approaches have been developed [6]. The "classical" porous medium approach [5] does not distinguish between individual channels and uses a single porous medium region instead. In this approach, resistance coefficients in the axial direction are used to represent losses experienced by the flow in the axial direction due to friction losses in the channels. Resistance coefficients in other two directions are set to very high values to ensure that the flow inside the monolith region is unidirectional. Since in this case the velocity inside the monolith region does not change with the axial coordinate, it is possible to "condense" the monolith in the axial direction and adjust the resistance coefficients correspondingly so that the total flow losses in the axial direction remain the same. This approach, called "condensed monolith approach", is described in detail in [6].

Here, the monolith has been modelled as a porous medium, using the “condensed” monolith approach in order to reduce mesh size and computational time. A comparison between the full domain and the one used with the condensed monolith approach is shown in Figure 2. The whole porous medium region length, for both L_1 = 27 mm and L_2 = 100 mm, is reduced to 2 mm in the condensed monolith case. The prescribed pressure drop has been scaled by the length factor, as explained in the next section. As a consequence, the number of cells used to discretize the porous medium region is reduced. As an indication, for the case of the 27 mm length, about 200000 cells are required to model all the channels [6], while with the condensed porous medium approach used in the current study, only 48850 cells are used.

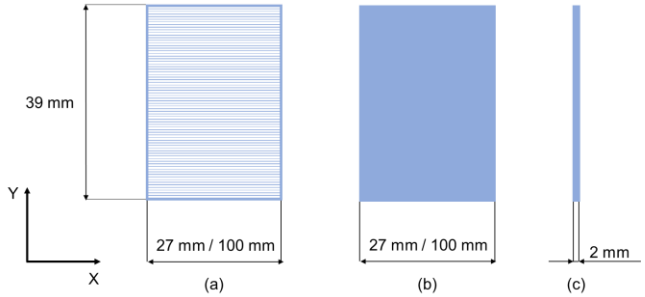

Figure 2. Monolith models comparison. Side view of the individual channels model (a), porous medium model of the full region (b) porous medium model with the condensed monolith approach (c).

Two different models for the pressure drop prediction have been compared. The first one is based on the expression

$$\Delta p/L=\alpha u+\beta u|u|, \tag{1}$$

where Δp is the pressure drop, L is the length of the monolith, u is the axial velocity at the monolith entrance, α is the viscous resistance coefficient and β is the inertial resistance coefficient, determined experimentally.

A more general prediction for the pressure drop, commonly adopted in automotive applications [8], is the correlation proposed by Shah [7] describing pressure losses in a channel with developing laminar flow:

$$\Delta p^{*}=\frac{\Delta p}{\rho u^{2}/2}=\left(f_{app}\mathrm{Re}\right)(4x^{+}). \tag{2}$$

In the above, the non-dimensional pressure drop Δp^{*} is calculated as a function of the apparent Fanning friction factor f_{app}, the Reynolds number Re based on the hydraulic diameter of the channel and the mean axial velocity in the duct, and the non-dimensional axial coordinate based on the channel hydraulic diameter H_d as reference length:

$$x^{+}=x/(H_d\mathrm{Re}). \tag{3}$$

The semi-empirical expression for the $f_{app}\mathrm{Re}$ proposed by Shah is

$$f_{app}\mathrm{Re}=\frac{3.44}{\sqrt{x^{+}}}+\frac{(f\mathrm{Re})+\frac{K(\infty)}{4x^{+}}-3.44/\sqrt{x^{+}}}{1+C(x^{+})^{-2}} \tag{4}$$

In this study, the constant values derived for a square channel have been used, namely: fanning friction factor fRe = 14.227, incremental pressure drop number $K(\infty)=1.43$ and constant $C=0.00029$.

Shape function

In the classic porous medium formulation, the axial resistance in the monolith depends only on the local superficial velocity as described by equation (1) or (2) or a similar expression. High resistance coefficients are used in the other directions to ensure that the flow is unidirectional. This causes flow redistribution upstream of the monolith, and usually results in flattening of the overall profile. However, the information about flow split between individual channels is lost.

The approach proposed in the current study, referred in the next sections as “modified approach”, prescribes a variable resistance across the monolith based not only on the flow velocity, but also on the channel geometry. A function describing the geometrical parameters of the monolith is introduced to scale the porous medium resistance, based on the hydraulic diameter H_d and the width of the monolith walls w, as shown in Figure 3.

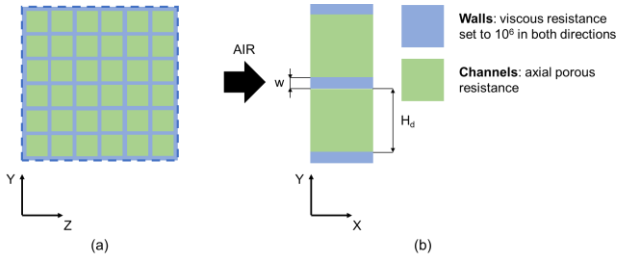

Figure 3. Schematic representation of a section of the monolith channels. Cross section (a), side view (b).

A custom field function called “Shape Function” (SF), has been created in the CFD software StarCCM+ to replicate the geometry of the monolith, with values set to 1 inside the channel walls, and zero elsewhere. The shape function is then used to modify the resistance coefficients of the porous medium, adding high resistance inside the walls.

Since Eq. (1) is based on the superficial velocity, and in the new formulation the actual mean channel velocity is used, the resistance coefficients for the porous region are scaled by the nominal Open Frontal Area of the monolith (OFA), as well as the length ratio to accommodate the fact that the monolith is "condensed" length-wise. For example, the viscous resistance coefficient α in equation (1), becomes α_{mod}

$$\alpha_{\mathrm{mod}}=\alpha_{\mathrm{exp}}\cdot\mathrm{OFA}\cdot\frac{L_{\mathrm{exp}}}{L_{\mathrm{sim}}}+\mathrm{SF}\cdot 10^{6}. \tag{5}$$

Here, α_{exp} is the viscous resistance coefficient determined from experiments, $\mathrm{OFA}=0.8819$ is the open frontal area factor of the monolith used in the current study, the factor $\frac{L_{exp}}{L_{sim}}$ accounts for the condensed monolith approach, scaling the experimental length of the monolith (L_{exp}) by the length of the porous region of the numerical model L_{sim}.

The coefficients calculated from the pressure drop formulation (1) or (5) are then used to prescribe the inertial and viscous resistance in the porous region. The corresponding porous resistance tensor is calculated and added as a sink in the momentum equation [16].

One of the advantages of the proposed model is the flexibility of the “Shape Function”. The geometry of the device can, indeed be easily modified by adjusting the function, without modifying the domain in the simulation process. This can be used for more complex cases, for example an asymmetrical configuration with soot and ash deposits considered [17].

Optimization function

The flow maldistribution upstream monoliths [18, 19] and heat exchangers [20] can significantly alter their performance. In order to optimize the velocity distribution inside the monolith channels, a simple algorithm is proposed that resizes the channel hydraulic diameter depending on the velocity entering it.

A first solution for the flow distribution is obtained imposing a constant channel diameter. The mean velocity for each channel is calculated and compared with the overall mean velocity at the monolith exit. The ratio between the mean velocity in the channel and

the overall mean velocity is the parameter used to determine if the channel diameter should be increased or decreased. A limit on the growth of the channel between each optimization step is set to 10%. The new solution is then calculated with the modified channel size distribution, until the uniform flow across all the channels is achieved.

The optimisation macro has been written in Java, in order to be integrated with StarCCM+, but can be extended to other applications and geometries and adapted to other CFD packages.

Results

To assess performance of the approach based on the shape function, the results are first compared with the "classic" porous medium approach based on Eq. (1) with the viscous and the inertial resistance coefficients determined from the experiments as reported in Table 1.

Table 1. Viscous and inertial resistance coefficients for the porous medium determined experimentally.

Monolith length [mm]	Viscous resistance coefficient (α) [kg/m^{3}s]	Inertial resistance coefficient (β) [kg/m^4]
27	734.48	14.053
100	259.5	19.806

The velocity profile downstream of the monolith is often used for assessment of monolith performance. Upstream of the monolith the flow features a velocity peak near the axis because flow separates on entry to the diffuser forming a central jet (Figure 4). As the jet approaches the monolith it spreads, diverting flow towards the side wall where it then either enters the monolith, thus causing the secondary peak shown in Figure 4, or it recirculates within the diffuser. Comparison of the normalised velocities at the outlet section for the inlet Reynolds number of 22000 and the monolith length of 27 mm (Figure 4) shows a good agreement between the two approaches.

The velocity is normalised by the mean outlet velocity from the simulations, equal to 2.72 m/s for Re = 22000 and 7.41 m/s for Re = 60000.

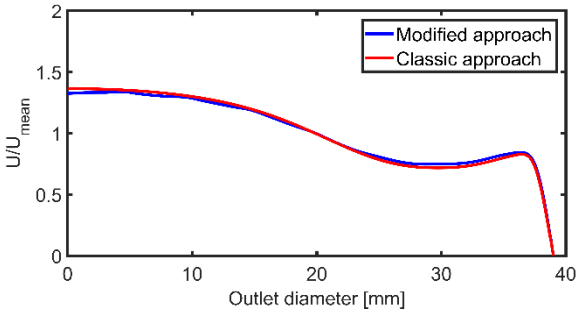

Figure 4. Non-dimensional velocity at the outlet section, classic approach (red line) and modified approach (blue line). Monolith length 27 mm, Re=22000.

With the modified porous medium approach, the jets exiting the channels are clearly visible downstream the monolith section (Figure 5b), while with the classic porous medium approach the jets are not captured by the simulation (Figure 5a).

Similar considerations can be made for the higher mass flow rate case, Figure 6 and Figure 7. A good agreement between the two approaches in the prediction of the downstream velocity is achieved.

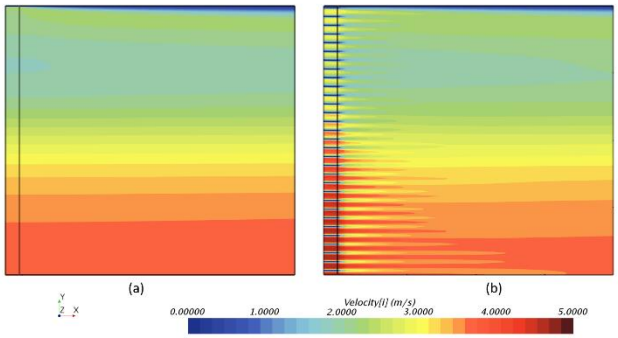

Figure 5. Axial velocity contours downstream the monolith. Classic approach on the left (a), modified approach on the right (b). Re =22000, monolith length 27 mm.

It can be seen from Figure 6 and Figure 7 that the jets exiting the monolith are not completely mixed downstream of the monolith section. This is one of the known limitations of the RANS modelling approach used, but the velocity oscillations observed in the outlet velocity are within 4% of the maximum velocity. This will be further investigated in future studies.

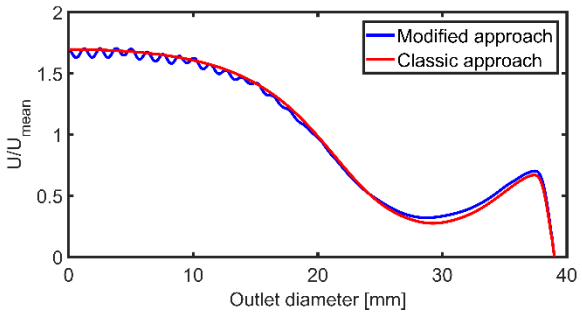

Figure 6. Non-dimensional velocity at the outlet section, classic approach (red line) and modified approach (blue line). Monolith length 27 mm, Re=60000.

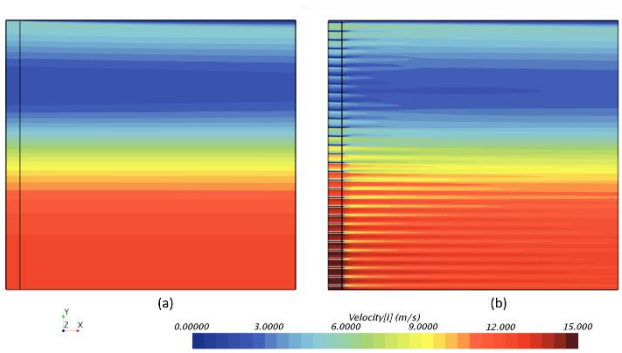

Figure 7. Axial velocity contours downstream the monolith. Uniform resistance on the left (a), modified resistance on the right (b). Re =60000, monolith length 27 mm.

The pressure loss across the monolith is higher with the use of the shape function, with an increase in pressure drop between 6% and 14% for the higher and lower inlet Reynolds number considered.

Unfortunately, no experimental measurements were available for comparison, so it is difficult to judge which model performed better.

Similar results have been obtained for the monolith of 100 mm length. The velocity profiles at the outlet section for the inlet Re = 22000 are shown in Figure 8, while the ones for the inlet Re = 60000 are shown in Figure 9.

Here, the pressure drop is also higher for the case with modified resistance: a 7% increase with the higher mass flow rate and a 12% increase with the lower mass flow rate.

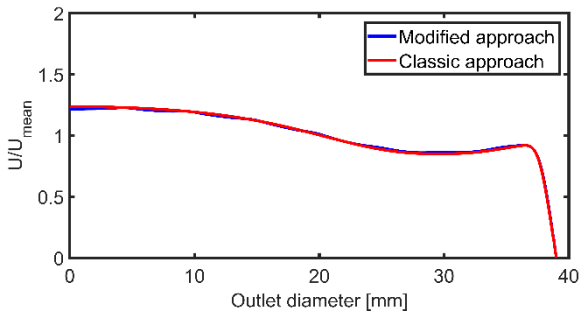

Figure 8 Non-dimensional velocity at the outlet section, classic approach (red line) and modified approach (blue line). Monolith length 100 mm, Re = 22000.

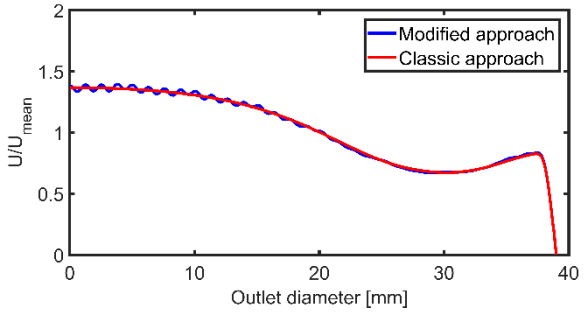

Figure 9. Non-dimensional velocity at the outlet section, classic approach (red line) and modified approach (blue line). Monolith length 100 mm, Re = 60000.

Prediction of downstream turbulence

One of the main aims of the current study was to assess the limitations of the classic porous medium approach in predicting turbulence properties downstream the monolith. The turbulence intensity (T_i) 30 mm downstream of the monolith was defined as

$$T_i = \frac{u'}{\bar{U}} \tag{6}$$

where u' is the velocity fluctuation and $\bar{U}$ is the mean velocity at the section. The velocity fluctuation u' has been computed as

$$u' = \sqrt{\frac{2}{3}k} \tag{7}$$

where k is the turbulent kinetic energy.

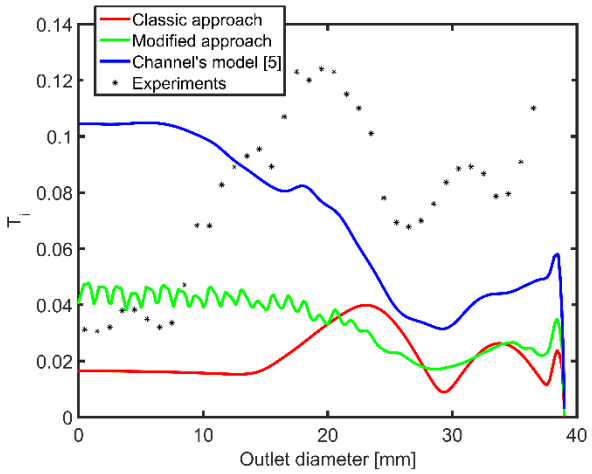

Figure 10. Turbulence intensity downstream the monolith. Classic approach (red line), modified approach (green line), Channel's model [6] (blue line), experiments (black dots). Inlet Re =60000, monolith length = 27 mm.

The proposed model shows a good agreement with the measured turbulence intensity near the axis of the diffuser (Figure 10). Further comparison has been made with the individual channel model by Porter et al. [6]. A similar trend in the distribution of the turbulence intensity can be seen for the proposed approach and the individual channel model (Figure 10). The classic porous medium approach results in under-estimation of the turbulence intensity near the diffuser axis, but seems to better capture the turbulence redistribution near the wall, due to the increased shear stress in that region.

This aspect is hardly surprising, since, as previously mentioned, different length scales are involved in the flow exiting the monolith and the turbulence model used for the simulation is a RANS eddy viscosity model [21].

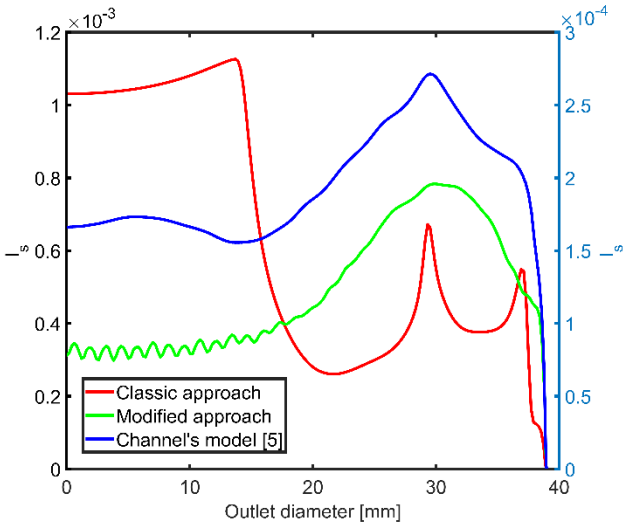

Figure 11. Turbulence length scale downstream the monolith comparison. Classic approach (red line) – left axis, modified approach (green line) and individual channel model [6] (blue line) – right axis.

This is confirmed by analysis of the turbulence length scale l_T extracted from the numerical model as

$$l_T = C_\mu \frac{k^{\frac{3}{2}}}{\varepsilon}, \quad (8)$$

in which C_μ=0.09 is one of the model's constants, k is the turbulent kinetic energy and ε is the turbulent dissipation. The results presented in Figure 11 clearly show that with the classic porous medium approach (red line) the modelled length scale is at least one order of magnitude higher than that predicted by the individual channel model (blue) or the modified resistance model (green). This confirms that with a classical porous medium approach model, only the macroscopic changes of the flow structures can be modelled, as confirmed by the good agreement with the first order properties, such as velocity (Figure 12) and pressure.

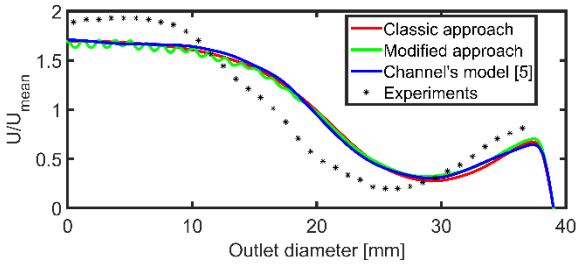

Figure 12. Outlet velocity comparison. Classic approach (red line), modified approach (green line), Channel's model [6] (blue line), experiments (black dots). Inlet Re =60000, monolith length = 27 mm.

Resistance based on Shah's correlation

Experimental pressure drop measurements are widely accepted as more suitable for determining porous and viscous resistance coefficients, because of uncertainties in channel hydraulic diameter values, and extra losses associated with the flow through a monolith (for example, contraction/expansion losses). However, these need to be repeated if monolith properties (e.g. length or hydraulic diameter) are changed.

In order to study the effect of changing monolith geometry, we first assess the performance of the Shah's correlation (2). The comparison with the experimental measurements obtained using uniform flow upstream the monolith is shown in Figure 13 and Figure 14. The pressure drop differences are summarised in Table 2, comparing the difference between the experiments and Shah's correlation assuming that the velocity upstream the monolith is uniform and equal to the mean value at the monolith surface. The comparison between the results of the simulations is also reported for both cases, showing a similar trend. Although there is a considerable difference between the experiments and Shah's correlation, especially for lower mass flow rates, Shah's correlation is used in the next section to demonstrate the optimisation procedure. Any other improved correlation that links channel hydraulic diameter to the pressure loss can be used instead. Note also that the experimental data curve is obtained by fitting a limited number of measurement points, and therefore has limited accuracy, especially for lower mass flow rates.

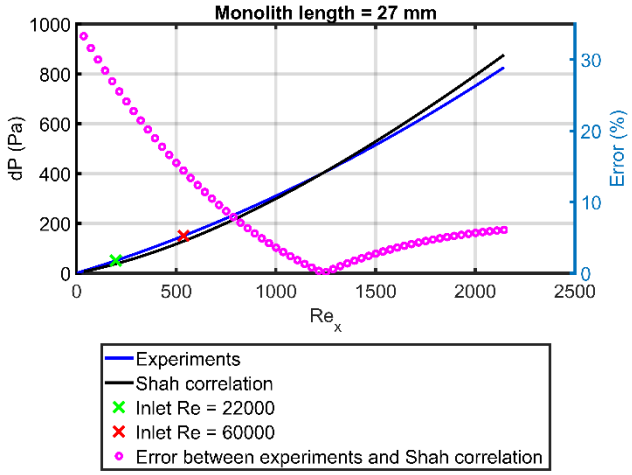

Figure 13. Comparison between the experimental pressure drop (blue line) and the pressure drop predicted with Shah's correlation (black line) for uniform flow at the monolith inlet. Mean velocity at the monolith surface for inlet Re=22000 (green cross), mean velocity at the monolith surface for inlet Re=60000 (red cross).

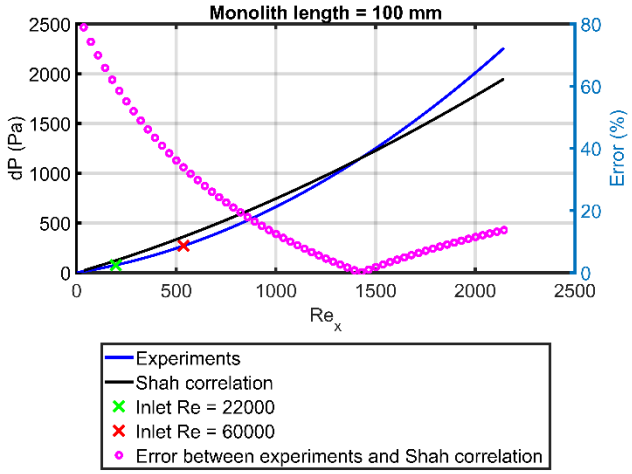

Figure 14. Comparison between the experimental pressure drop (blue line) and the pressure drop predicted with Shah's correlation (black line) for uniform flow at the monolith inlet. Mean velocity at the monolith surface for inlet Re=22000 (green cross), mean velocity at the monolith surface for inlet Re=60000 (red cross).

To ensure that the difference between the experimental resistance coefficients and Shah's correlation does not considerably affect the simulation results, Shah's correlation (2) has been used for prescribing resistance properties of the porous medium, combined with the shape function. The results for the monolith length of 27 mm are shown in Figure 15 for the inlet Re = 22000 and in Figure 16 for the inlet Re = 60000, while the ones for the longer monolith length of 100 mm are shown in Figure 17 for the inlet Re = 22000 and in Figure 18 for the inlet Re = 60000.

The agreement between the outlet velocity profiles has been achieved in all the cases, with the error within 3%. This justifies using the empirical correlation (2) for cases where experimental data is unavailable, such as the optimisation study presented below.

Table 2. Pressure drop comparison: difference between experimental curve and Shah's correlation ("theoretical") using the mean velocity at the monolith entrance and difference between numerical results using the experimental coefficients and Shah correlation ("simulations").

Inlet Re	Monolith length [mm]	Mean velocity [m/s]	Pressure drop difference (theoretical)	Pressure drop difference (simulations)
22000	27	2.75	-24.12 %	-17.65 %
	100	7.50	+60.23 %	+48.52 %
60000	27	2.75	-14.42 %	-2.27 %
	100	7.50	+33.91 %	+22.44%

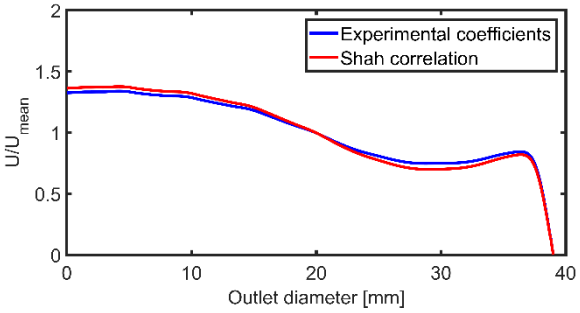

Figure 15. Non-dimensional velocity at the outlet section, modified resistance using Shah's correlation (red line) and modified resistance from experimental data (blue line). Monolith length 27 mm, Re = 22000.

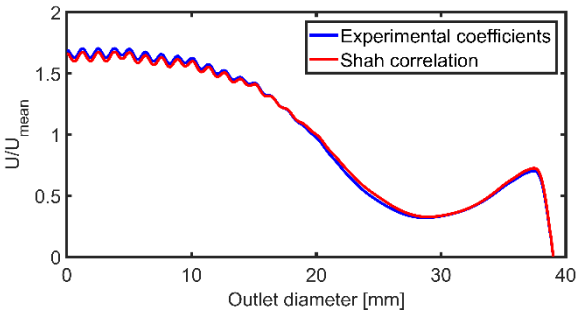

Figure 16. Non-dimensional velocity at the outlet section, modified resistance using Shah's correlation (red line) and modified resistance from experimental data (blue line). Monolith length 27 mm, Re = 60000.

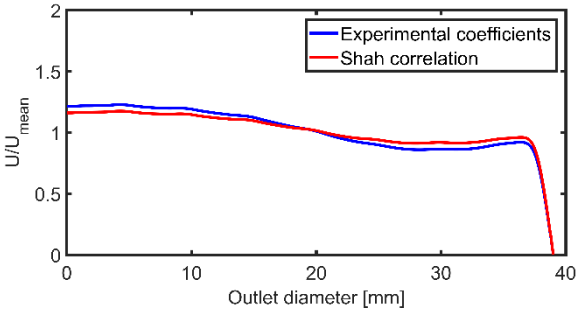

Figure 17. Non-dimensional velocity at the outlet section, modified resistance using Shah's correlation (red line) and modified resistance from experimental data (blue line). Monolith length 100 mm, Re = 22000.

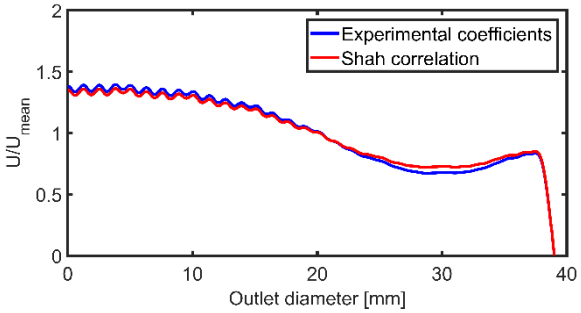

Figure 18. Non-dimensional velocity at the outlet section, modified resistance using Shah's correlation (red line) and modified resistance from experimental data (blue line). Monolith length 100 mm, Re = 60000.

Channel optimization

The algorithm proposed for the channels optimisation has been applied to the 27 mm monolith, using the two inlet Re of 22000 and 60000, referred as Case 1 and Case 2. More uniform flow was obtained by changing the resistance across the monolith with larger channels placed near the wall. The relatively higher resistance in the centre of the monolith thus forced more flow away from the centreline, flattening the flow profile. A comparison between the axial velocity contours is presented in Figure 19 and Figure 20. For both figures, the simulations with uniform channel size distribution is shown on the left, while the simulation results with optimised geometry are shown on the right.

In order to assess the overall performance of the new distribution, the pressure drop difference and the uniformity index are compared in Table 3. The uniformity index (UI) has been calculated at the outlet section of the domain, using the following expression:

$$UI=1-\frac{\sum_i |U_i-\bar{U}|A_i}{2|\bar{U}|\sum_i A_i}, \quad (9)$$

in which U_i is the mean axial velocity in the cell i, A_i is the cell area and $\bar{U}$ is the mean axial velocity in the section. The original (non-optimised) UI for the inlet Re = 22000 with constant channel diameter was 0.87, while the UI for the inlet Re = 60000 with constant channel diameter was 0.76.

As expected, the optimised channel size distribution results in a reduction of the total pressure drop across the monolith and higher uniformity indices for both Case 1 and Case 2 (Table 3).

This demonstrates how the monolith channel size distribution can be improved for a fixed mass flow rate. In applications, however, the mass flow is usually variable. Therefore, optimisation for a range of mass flow rates would ideally be required.

To assess whether channel distribution optimised for one mass flow rate can be used for a different mass flow, two further simulations have been carried out. The first one (Case 3) is using the channel size distribution obtained in Case 2 for an inlet Re = 22000, and the second one (Case 4) is using the channel size distribution obtained in Case 1 for an inlet Re=60000.

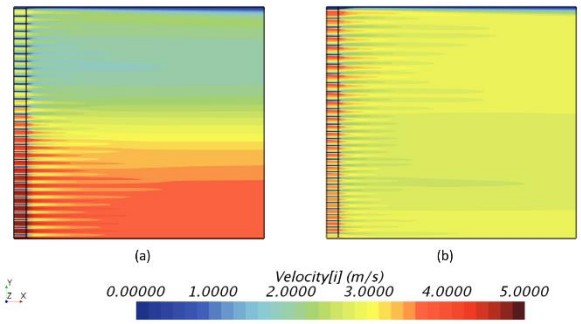

Figure 19. Axial velocity contours downstream the monolith. Uniform distribution on the left (a), optimised distribution on the right (b). Re =22000, monolith length 27 mm.

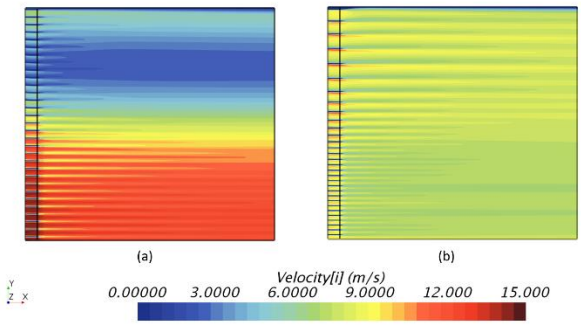

Figure 20. Axial velocity contours downstream the monolith. Uniform distribution on the left (a), optimised distribution on the right (b). Re =60000, monolith length 27 mm.

Table 3. Optimization results: pressure drop difference between optimised channel size distribution and equal channel size distribution (Unif.) and UI for each case.

	Re = 22000			Re = 60000		
Case	Unif.	1	3	Unif.	2	4
Δp	-	-1.6%	-16%	-	-4.3%	+3%
UI	0.87	0.98	0.82	0.76	0.97	0.87

The resulting changes in total pressure loss and uniformity indices are listed in Table 3. A considerable pressure drop reduction has been obtained in Case 3, in which the channel's distribution optimised for Re = 60000 has been used with lower Re=22000 at the inlet, with a slight reduction of the UI, compared to the constant channel diameter case. The opposite trend is observed in Case 4, in which the distribution optimised for the lower Re is used with a higher Re at the inlet. The pressure drop is slightly increased, but the UI is considerably better than the one with constant channel diameter case.

This trend seems to suggest that the optimization of the channel's diameter obtained for one particular mass flow rate upstream, can be beneficial in terms of either pressure drop reduction, with lower mass flow rates, or increased uniformity index, with higher mass flow rates. This aspect will be further investigated in future studies.

Conclusions

A new approach for modelling multi-channel devices based on the porous medium approach has been proposed. The main advantages of the classic approach, such as good prediction of the downstream velocity and low computational expenses, are kept with the proposed modification.

The approach has been used for modelling two-dimensional flow in a diffuser with an automotive catalyst. An improvement in the prediction of the downstream turbulence properties has been shown with the proposed modification, with respect to the classic porous medium approach. In particular, the single jets exiting the channels of the monolith can be captured by the proposed model, as well as turbulence generation associated with jet mixing, with a good agreement with 2D models that include the channels' geometry, published in literature [6].

The main limitations of the accuracy of the results with the experimental data have been assessed. The use of a RANS turbulence model based on the eddy viscosity hypothesis limits the prediction of the multiple turbulent length scales involved - in particular, the smaller scales associated with individual jet mixing downstream of the monolith, and larger scales associated with the global shear layer formed when the flow enters the expansion from the smaller inlet pipe. The model will therefore be tested with more complex turbulence models, such as Reynolds Stress Models and Large Eddy Simulation, in the next phase of the study.

The proposed approach will also be further tested prescribing variable resistance coefficients inside the monolith channels, based on quadratic, cubic or high-order laws.

Flexibility of the proposed model in the device geometry description has been demonstrated by implementing a channel size optimisation algorithm in order to improve flow uniformity. The results of the optimisation study have shown a considerable improvement of the flow uniformity index downstream the monolith and the total pressure loss across the monolith. Further numerical and experimental activities will be carried out, to extend the formulation to a three-dimensional case, to improve the optimization procedure and to better validate the model against experimental data.

References

1. Prithiviraj, M., and M. J. Andrews. "Three dimensional numerical simulation of shell-and-tube heat exchangers. Part I: foundation and fluid mechanics." Numerical Heat Transfer, Part A Applications 33.8 (1998): 799-816, doi: 10.1080/10407789808913967
2. Cornejo, Ivan, Petr Nikrityuk, and Robert E. Hayes. "Multiscale RANS-based modeling of the turbulence decay inside of an automotive catalytic converter." Chemical Engineering Science 175 (2018): 377-386, doi: 10.1016/j.ces.2017.10.004
3. Guardo, A., et al. "Influence of the turbulence model in CFD modeling of wall-to-fluid heat transfer in packed beds." Chemical Engineering Science 60.6 (2005): 1733-1742, doi: 10.1016/j.ces.2004.10.034
4. Su, C., Brault, J., Munnannur, A., Liu, Z. G., et al. (2019). "Model-Based Approaches in Developing an Advanced Aftertreatment System: An Overview" SAE Technical Paper. doi https://doi.org/10.4271/2019-01-0026
5. Benjamin, S. F., et al. "Modelling the flow distribution through automotive catalytic converters." Proceedings of the Institution of Mechanical Engineers, Part C: Journal of mechanical

engineering science 215.4 (2001): 379-383, doi: 10.1243/0954406011520779.
6. Porter, Sophie, et al. "An assessment of CFD applied to steady flow in a planar diffuser upstream of an automotive catalyst monolith." SAE International Journal of Engines 7.4 (2014): 1697-1704, doi: 10.4271/2014-01-2588
7. Shah, R. K. "A correlation for laminar hydrodynamic entry length solutions for circular and noncircular ducts." Journal of Fluids Engineering 100.2 (1978): 177-179, doi: 10.1115/1.3448626.
8. Abu-Khiran, Esam, Roy Douglas, and Geoffrey McCullough. "Pressure loss characteristics in catalytic converters." SAE transactions (2003): 2123-2134, doi: 10.4271/2003-32-0061.
9. Hayes, R. E., et al. "CFD modelling of the automotive catalytic converter." Catalysis today 188.1 (2012): 94-105, doi: 10.1016/j.cattod.2012.03.015.
10. Cornejo, Ivan, Petr Nikrityuk, and Robert E. Hayes. "Turbulence generation after a monolith in automotive catalytic converters." Chemical Engineering Science 187 (2018): 107-116, doi: 10.1016/j.ces.2018.04.041.
11. Gao, Xi, Ya-Ping Zhu, and Zheng-hong Luo. "CFD modeling of gas flow in porous medium and catalytic coupling reaction from carbon monoxide to diethyl oxalate in fixed-bed reactors." Chemical Engineering Science 66.23 (2011): 6028-6038, doi: 10.1016/j.ces.2011.08.031.
12. Kuwata, Yusuke, Kazuhiko Suga, and Yota Sakurai. "Development and application of a multi-scale k–ε model for turbulent porous medium flows." International Journal of Heat and Fluid Flow 49 (2014): 135-150, doi: 10.1016/j.ijheatfluidflow.2014.02.007.
13. Ruiz-Morales, J. C., et al. "Three dimensional printing of components and functional devices for energy and environmental applications." Energy & Environmental Science 10.4 (2017): 846-859, doi: 10.1039/C6EE03526D.
14. Thakkar, Harshul, et al. "3D-printed zeolite monoliths for CO2 removal from enclosed environments." ACS applied materials & interfaces 8.41 (2016): 27753-27761, doi: 10.1021/acsami.6b09647.
15. Williams, Jimmie L. "Monolith structures, materials, properties and uses." Catalysis Today 69.1-4 (2001): 3-9, doi: 10.1016/S0920-5861(01)00348-0.
16. CD-adapco, S. "STAR CCM+ User Guide Version 12.04." CD-Adapco: New York, NY, USA (2017).
17. Wang, Yujun, et al. "Performance of Asymmetric Particulate Filter with Soot and Ash Deposits: Analytical Solution and Its Application." Industrial & Engineering Chemistry Research 57.46 (2018): 15846-15856. doi: 10.1021/acs.iecr.8b02848
18. Benjamin, S. F., Z. Liu, and C. A. Roberts. "Automotive catalyst design for uniform conversion efficiency." Applied Mathematical Modelling 28.6 (2004): 559-572, doi: 10.1016/j.apm.2003.10.008.
19. Agrawal, Gaurav, et al. "Modeling the effect of flow mal-distribution on the performance of a catalytic converter." Chemical engineering science 71 (2012): 310-320, doi 10.1016/j.ces.2011.12.041.
20. Singh, Sanjay Kumar, Manish Mishra, and P. K. Jha. "Nonuniformities in compact heat exchangers—scope for better energy utilization: A review." Renewable and Sustainable Energy Reviews 40 (2014): 583-596, doi: 10.1016/j.rser.2014.07.207.
21. Pope, Stephen B. "Turbulent flows." (2001), doi: 10.1088/0957-0233/12/11/705.

Contact Information

padulag@uni.coventry.ac.uk

Definitions/Abbreviations

CFD	Computational Fluid Dynamics
RANS	Reynolds Averaged Navier-Stokes
L	Monolith length
H_d	Hydraulic diameter
Δp	Pressure drop
α	Viscous resistance coefficient
β	Inertial resistance coefficient
u	Velocity at monolith entrance
Δp^*	Non-dimensional pressure drop
ρ	Flow density
f_{app}	Apparent Fanning friction factor
Re	Reynolds number
x^+	Non-dimensional axial coordinate
fRe	Fanning friction factor
$K(\infty)$	Incremental pressure drop number
C	Constant (Shah's correlation)
α_{mod}	Modified viscous resistance coefficient
OFA	Open frontal area of the monolith
T_i	Turbulence intensity
u'	Velocity fluctuation
$\bar{U}$	Mean velocity in the section
k	Turbulent kinetic energy
l_T	Turbulent length scale
C_μ	Turbulent model constant
ε	Turbulent dissipation
UI	Uniformity index